SHOCK EFFECTS ON OLIVINE STRUCTURE AND SLIP SYSTEMS IN MARTIAN DUNITE NORTHWEST AFRICA 2737. Y. Li[1,2], P.J.A. McCausland[1,2], R.L. Flemming[1,2]
[1]Department of Earth Sciences and [2]Institute for Earth and Space Exploration, Western University, London, ON, Canada N6A 5B7. *yli2889@uwo.ca*

Introduction: Martian chassignite Northwest Africa (NWA) 2737 is the second known meteorite sample representing Martian dunitic cumulates [1,2]. NWA 2737 crystallized about 1.3 Ga ago from basaltic magma along with Chassigny and the other chassignite sample Northwest Africa 8694 [3,4,5].

Olivine is the primary mineral phase in NWA 2737 with minor augite and spinel, and accessory amounts of feldspathic and granitic clasts [1,2,5]. The sample appears to be heavily shocked, based on observations of strongly brown-stained olivine (likely due to inclusions of nanophase iron or iron metal alloy [6,7]), appearance of planar fractures in olivine, and partial transition of olivine to its high-pressure metastable polymorph ringwoodite [7,8]. Chassigny and the two chassignite samples are classified as Martian cumulates because of their cumulate-like textures and the high model abundance of olivine [2,3,4]. However, a study on NWA 8694 revealed it had no directional fabric or lattice preferred orientation (LPO) patterns [e.g., 3] as is typically found in terrestrial cumulate rocks [9,10,11].

To further contribute to the topic and to investigate Martian upper mantle, in our work we examine a thick section sample of NWA 2737 by *in-situ* micro-X-ray diffraction (μXRD) and electron backscattered diffraction (EBSD). Shock induced subdomain misorientation is observable by μXRD and can be quantitatively calculated to reflect the degree of shock. Potential slip systems and intragranular orientation formed and modified by burial pressure and/or shock events can be obtained by EBSD. In these preliminary results, we focus on shock effects on individual grains and how the crystal lattices react to the deconstructive shock wave under the extreme strain rate.

Methods: This study used the Bruker D8 Discover μXRD at Western University with a Co Kα X-ray source (λ Co $K\alpha_1$ = 1.78897 Å) and Vantec-500 detector, with General Area Detector Diffraction System (GADDS) software, which obtains 2D diffraction patterns similar to Debye-Scherrer film. Shock can be indicated by X-ray diffraction textures on 2D images. Deformation of single crystals is observed as strain-related mosaicity (SRM) or misorientation of subdomain 'mosaic blocks' in the crystal due to non-uniform strain (plastic deformation), recorded by 2D XRD as streaks or asterism along the arc of Debye rings (chi dimension, χ) for each lattice plane with Miller index (hkl) [12-16]. A positive trend of shock degrees and Full-Width-Half Maximum measured on simple peaks integrated from 2D XRD patterns along Debye rings has been found and well-discussed by previous works [13-16]. In this work, quantitative SRM is done by a Matlab program Best Fit for Complex Peaks (BFCP) coded by Li et al. (2020). It measures the sum of Full-Width-Half Maximum (∑(FWHMχ) of complex peaks integrated from XRD patterns [17].

2D XRD data for all samples were collected in omega scan mode. To maximize collecting area, we used θ1 = 14.5°, θ2 = 20.5° and ω = 10° for Frame 1; θ1 = 37°, θ2 = 43° and ω = 16° for Frame 2. Each frame was collected for 1 hour, making 2 hours per target. All the peaks measured by BFCP used pseudo-Voigt function.

Electron-backscattered diffraction (EBSD) was performed at McMaster University, Canadian Centre for Electron Microscopy. Data is collected by JEOL JSM-7000F with a Schottky field emission gun and integrated Oxford Instruments X-Max^n 50 mm^2 EDS detector and Nordlys II EBSD Camera, providing resolution as fine as 1.2 nm at 30 keV and 3.0 nm at 1 keV. Data is processed by AZtec EDS/EBSD software plus HKL Channel EBSD software for the simultaneous acquisition of elemental and crystal orientation information. In this study, given the large olivine grains as targets, we collected electron diffraction data at a spacing of 2-3 μm depending on the size of grains to optimize collecting time and data resolution.

Results: NWA 2737 is primarily composed by forsterite olivine with minor amount of pyroxene confirmed by micro-X-ray diffraction. The coarse-grained stained olivine dominantly shows moderate to long diffraction streaks along the Debye Rings (Figure 1), indicating misoriented subdomains of crystal lattices consistent with shock-generated non-uniformly distributed strain. Quantitative SRM analysis measured 40 peaks integrated from XRD patterns, and the mean ∑(FWHMχ) is 11.22° ± 2.89°. Top 25% of ∑(FWHMχ), reflecting the most shocked grains, is 15.7 ° ± 1.18 °. According to the olivine SRM shock scheme developed from ureilites [18], NWA 2737 has shock stage of S5-S6 equivalent to shock pressure over 30GPa to 55GPa. This shock stage result is consistent with previous work [1-5].

Preliminary EBSD analysis focuses on large olivine grains. In Figure 2, the green color corresponds with the phase olivine whereas black indicates no identified phase, due to: 1) uneven polished surface (Figure 2A and 2B) or 2) missing mineral phases (Figure 2C). Data for identification was collected only when mean angular deviation (MAD) was smaller than 1°.

Relatively large-angle boundary contacts (>15°) are common between olivine grains and can be visually observed on Euler color maps. Intragrain angles within large olivine grains are between 0.5° to 2.6° representing the misorientation among subdomains. This observation is consistent with XRD, observed as a mosaic spread along Debye rings, forming streaky patterns (Figure 1). Possible mechanical twining is also observed on one target (Figure 2C), with misorientation angles from 0.5 ° to 4.5 ° (purple to brown).

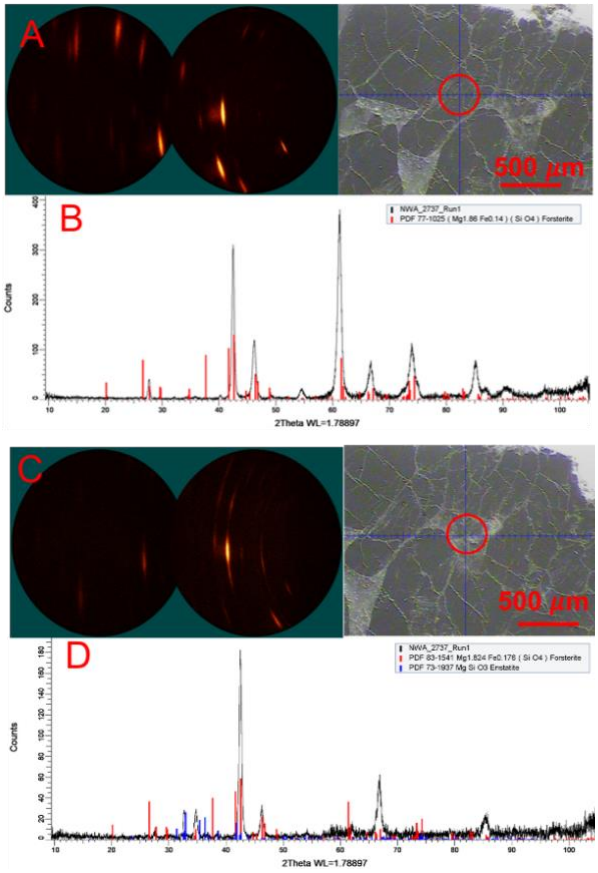

Figure 1. Example of XRD Patterns. Representative 2D XRD patterns and target images for two olivine grain targets in NWA 2737. The red circle marks the XRD targeting area which is 300 microns. **1A** shows the dominant streak patterns along the Debye ring in 2D XRD, indicating the misorientation of subdomains due to shock. **1B** shows the integrated diffraction pattern for mineral phase matching. All the diffraction peaks (black) match with standard forsterite olivine ICDD card (red). **1C** shows a similar streak pattern along Debye rings for a second target. **1D** shows the integrated diffraction peaks (black) match with forsterite olivine (red) and minor amount of pyroxene (blue).

Acknowledgements: PJAM and RLF acknowledge research funding support from the NSERC – Discovery program. Chris Herd (University of Alberta) kindly provided the sample on loan. Christopher Butcher at McMaster assisted with EBSD data collection.

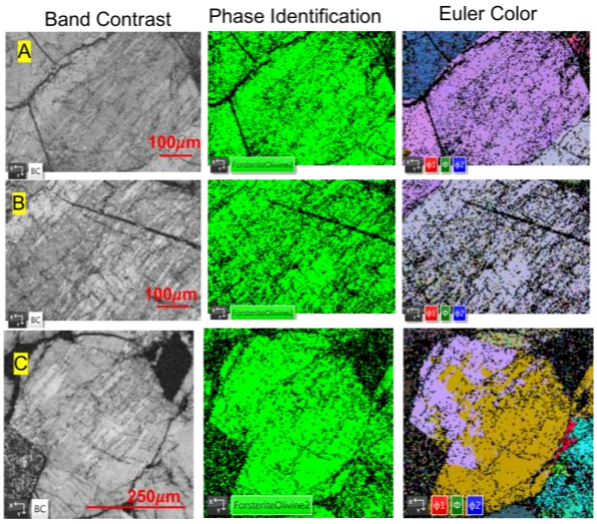

Figure 2. Selected EBSD Targets and Preliminary Results. From left to right, it shows band contrast, phase identification, and Euler color images. In the Phase Identification images, green color indicates phase identified as olivine, and black color means no phase identification. The Euler color images visually tell the orientation differences constructed by red, green, and blue colors representing Euler angle **φ**1, **Φ**, and **φ**2. Orientation variation is commonly observed between grains (**2A**) forming relatively large angle grain boundary (>15 °). In **2C**, two orientations (~4.5 °) are observed possibly due to mechanical twining of olivine.

References [1] Beck, P., et al. (2006) Geochimica et Cosmochimica Acta, 70: 2127–2139. [2] Bläß, U.W., et al. (2010) Earth and Planetary Science Letters, 300: 255–263. [3] Tkalcec, B. J., and Brenker, F. E. (2019) Meteoritics & Planetary Sci., 54(2), 267-279. [4] Misawa, K., et al (2006). Earth and Planetary Science Letters, 246(1-2), 90-101. [5] Treiman, A.H., et al. (2007) J. of Geophysical Research: Planets, 112. [6] Reynard, B., et al. (2007) *Earth and Planet. Sci. Letters*, *262*(1-2), 37-49. [7] Pieters, et al., (2008) J. of Geophysical Research: Planets, 113. [8] Van de Moortèle, B., et al. (2007) Earth and Planet. Sci. Letters, 261: 469–475. [9] Mainprice, D., et al. (2005). Nature, 433: 731–733. [10] Ohuchi, T., et al. (2011) Earth and Planet. Sci. Letters, 304: 55–63. [11] Raterron, P. et al. (2007). Am. Mineral., 92: 1436–1445. [12] Flemming R. L. (2007) *Can. J. Earth Sci.*, 44, 1333–1346. [13] Hörz F. and Quaide W. (1973) *Earth, Moon, and Planets*, 6, 45–82. [14] Vinet N. et al. (2011) *Am. Mineral.*, 96, 486-497. [15] Pickersgill A. E. et al. (2015) *Meteoritics & Planet. Sci.*, 50, 1851–1862. [16] Jenkins, L. E. et al. (2019) *Meteoritics & Planet. Sci.*, 54, 902-918. [17] Li, Y., et al. (2020) Comp. & Geosci., 144, 104572. [18] Li, Y., et al. (2021), Meteoritics & Planet. Sci. (accepted)